

Excess charge delocalization in organic and biological molecules: some theoretical notions

Lluís Blancafort · Miquel Duran · Jordi Poater ·
Pedro Salvador · Sílvia Simon · Miquel Solà ·
Alexander A. Voityuk

Received: 11 February 2009 / Accepted: 11 February 2009 / Published online: 7 March 2009
© Springer-Verlag 2009

Abstract Theoretical and computational investigations of the excess charge distribution (ECD) in molecular complexes have attracted considerable attention as ECD is closely related to electronic properties of organic semiconductors, such as the efficiency of photoinduced charge separation in organic solar cells and charge transport in DNA and proteins. In this paper, we analyze the ECD in several representative models on the basis of *ab initio* and DFT calculations. We consider how changes in the reorganization energy, electronic coupling and charge transfer energy affect the ECD in the systems. In particular, we compare ECD in π stacks of polycyclic aromatic hydrocarbons and DNA nucleobases. While the π interaction between subunits in the systems is similar in both cases, ECD is quite different: the excess charge is found to be completely delocalized over the hydrocarbon stacks but strongly confined to a single nucleobase in DNA stacks. We also discuss the effects of conformational fluctuations on ECD in the stacks. Finally, ECD in amino acids and its

dependence on the conformational changes are briefly considered.

Keywords Electron transfer · Charge delocalization · CASPT2 · DFT · Aromatic molecules · DNA

1 Introduction

Aromatic molecules and their stacks can be used as building blocks in molecular electronics [1–3]. Actually, fullerenes and their derivatives are already widely employed in solar cells (photovoltaic devices) [4] and may also be key elements for different electronic devices. Because of the biological relevance and potential use in nanotechnology, the electron transfer processes in DNA and proteins have also attracted great attention of both experimentalists and theoreticians [5].

Photochemical or electrochemical doping introduces charge carriers in the system; depending on the injected charge, two types of charge transfer (CT) can be activated: (i) hole transfer (HT), when a radical-cation state migrates within the system and (ii) excess electron transfer (EET), when a radical-anion state moves from one site to another.

The last 20 years have been very important for understanding CT mechanisms underlying in molecular electronics [6, 7]. The efficiency of CT as well as delocalization of an excess charge over the system depends critically on the electronic interactions between its subunits [8, 9]. Detailed discussion of how these CT processes can be described at the molecular level is given in excellent reviews [10, 11]. Three key parameters, the donor–acceptor energy gap ΔG , the electronic coupling V , and the reorganization energy λ , determine the probability of electron transfer in the nonadiabatic regime [11]. In many systems

Dedicated to Professor Santiago Olivella on the occasion of his 65th birthday and published as part of the Olivella Festschrift Issue.

Electronic supplementary material The online version of this article (doi:10.1007/s00214-009-0538-8) contains supplementary material, which is available to authorized users.

L. Blancafort · M. Duran · J. Poater · P. Salvador · S. Simon ·
M. Solà · A. A. Voityuk
Institut de Química Computational
and Departament de Química,
Universitat de Girona, 17071 Girona, Spain

A. A. Voityuk (✉)
Institució Catalana de Recerca i Estudis Avançats,
08010 Barcelona, Spain
e-mail: alexander.voityuk@icrea.es

of interest that comprise identical subunits, the energy gap is zero, and therefore, the excess charge mobility depends only on the reorganization energy λ and electronic coupling V [12]:

$$k = \frac{2\pi}{\hbar} V^2 \frac{1}{\sqrt{4\pi\lambda k_B T}} \exp[-\lambda/4k_B T] \quad (1)$$

In such cases, the interplay of V and λ determines directly the delocalization of the excess charge between donor and acceptor [13, 14]. Within a two-state model, the difference of the excess charge on subunits 1 and 2, $\Delta q = q_2 - q_1$, can be obtained from the following equation [14]:

$$\Delta q = \frac{1}{\sqrt{1 - (2V/\lambda)^2}} \quad (2)$$

Thus, Δq depends on the ratio of the reorganization energy and the coupling. From Eq. 2, we can derive the 90% of the excess charge will be confined to one of the subunits when $|V| < \lambda/5$, and the charge is essentially delocalized over both sites when $|V| > \lambda/2$. Delocalization of the charge reduces the intrinsic energy of the system, whereas the reorganization energy stabilizes the states with a localized excess charge.

The reorganization energy for CT comprises the internal and external contributions, $\lambda = \lambda_i + \lambda_e$. The internal reorganization energy is a function of the electronic structure of the molecule. For instance, the formation of the radical cation or radical anion of a polycyclic aromatic system requires a quite small internal reorganization energy (0.1 eV), whereas $\lambda_i = 0.3$ eV is found for nucleobases and aromatic amino acids. If the excess charge is localized on a few atomic centers, λ can be ~ 1 eV. The external reorganization energy is determined by relaxation of the environment and has been already considered in detail [12, 15]. Note that λ_e is often negligibly small for organic systems, while it is essential for CT in polar environment, e.g. in DNA and proteins.

In the present paper, we analyze the excess charge delocalization in several representative models and consider the interplay between the reorganization energy for detachment and attachment of an electron and the electronic structure of the systems.

2 Methods

2.1 Charge distribution

Within the Kohn–Sham (KS) approach, the excess charge distribution (ECD) in the ground state of a radical cation or radical anion can be derived using population analysis of

the appropriate KS orbitals of the neutral system, usually the HOMO and LUMO. In the excited state of the radical cation, the charge can be estimated using the corresponding coefficients in HOMO–1 (or a lower occupied MO). The ECD in the excited state of radical anion may be derived from LUMO+1 (or a higher MO). The atomic charges and overlap populations can be obtained by a number of standard methods. In case of the Mulliken population analysis, the excess charge on a fragment A in the ground state of the radical cation and anion can be estimated as

$$\begin{aligned} q_A^{\text{HOMO}} &= \sum_{\mu \in A} \sum_{\nu} c_{\mu, \text{HOMO}} S_{\mu\nu} c_{\nu, \text{HOMO}}^* = \sum_{\mu \in A} (P_{\text{HOMO}} S)_{\mu\mu} \\ q_A^{\text{LUMO}} &= \sum_{\mu \in A} \sum_{\nu} c_{\mu, \text{LUMO}} S_{\mu\nu} c_{\nu, \text{LUMO}}^* = \sum_{\mu \in A} (P_{\text{LUMO}} S)_{\mu\mu} \end{aligned} \quad (3)$$

where S is the overlap matrix of the basis set and the summation over μ is restricted to only those basis functions centered on atom A . For the DNA stacks, the charges were estimated by summing the CASSCF Mulliken charges on the bases.

Similarly, the overlap population of the HOMO and LUMO orbitals, accounting for the degree of sharing of the excess charge, can be obtained simply by

$$\begin{aligned} q_{AB}^{\text{HOMO}} &= 2 \sum_{\mu \in A} \sum_{\nu \in B} c_{\mu, \text{HOMO}} S_{\mu\nu} c_{\nu, \text{HOMO}}^* \\ q_{AB}^{\text{LUMO}} &= 2 \sum_{\mu \in A} \sum_{\nu \in B} c_{\mu, \text{LUMO}} S_{\mu\nu} c_{\nu, \text{LUMO}}^* \end{aligned} \quad (4)$$

A positive value of q_{AB}^{HOMO} can be understood as a weakening of the bonding interaction between atoms A and B by removing an electron from the HOMO. In the case of q_{AB}^{LUMO} , a negative value would imply a weakening of the bond induced by an electron attachment process.

Another approach is to perform the population analysis on the 3D space. In this case, a molecular quantity (such as the density) is decomposed into atomic contributions by integrating only over the part of the 3D space associated to each atom. For the ECD under the Koopmans' approximation, we can write

$$\begin{aligned} q_A^{\text{HOMO}} &= \int_A \rho_{\text{HOMO}}(\vec{r}) d\vec{r} = \int \rho_{\text{HOMO}}(\vec{r}) w_A(\vec{r}) d\vec{r} \\ q_A^{\text{LUMO}} &= \int_A \rho_{\text{LUMO}}(\vec{r}) d\vec{r} = \int \rho_{\text{LUMO}}(\vec{r}) w_A(\vec{r}) d\vec{r} \end{aligned} \quad (5)$$

where ρ_{HOMO} and ρ_{LUMO} are the orbital densities and $w_A(\vec{r})$ is an atomic weight factor that measures to which extent a given point of the space \vec{r} belongs to atom A . For a 3D space analysis, such as Bader's *Atoms in molecules* [16], the atomic domains are disjoint, i.e., the atomic weight function is 1 if the point of the space lies inside the atomic basin and 0 otherwise. In the Hirshfeld method [17]

and general fuzzy atom approach, the values of the atomic weight functions are close to 1 in the vicinity of the atom and monotonically decrease to 0 when moving apart from the atomic center. Various fuzzy atom approaches differ in the shape of the atomic weight factors but since the atomic domains are not disjoint, non-zero overlap populations analogous to Eq. 4 can be obtained by

$$\begin{aligned} q_{AB}^{\text{HOMO}} &= 2 \int \rho_{\text{HOMO}}(\vec{r}) w_A(\vec{r}) w_B(\vec{r}) d\vec{r} \\ q_{AB}^{\text{LUMO}} &= 2 \int \rho_{\text{LUMO}}(\vec{r}) w_A(\vec{r}) w_B(\vec{r}) d\vec{r} \end{aligned} \quad (6)$$

where the factor of 2 is included in order to account only for non-distinct atomic pairs.

2.2 Internal reorganization energy

The reorganization energy for ET reactions turns out to be a sum of the reorganization energies of the donor and acceptor sites. For ET between two identical subsystems S , $\lambda_i = 2\lambda_i(S)$. To estimate $\lambda_i(S)$, the following terms were computed: (1) the energy $E_0(S)$ of neutral S at its optimized geometry, (2) the energy $E_-(S^-)$ of the corresponding anion radical at its optimized geometry, (3) the energy $E_-(S)$ of the radical-anion state at the optimized geometry of the neutral molecule S , and (4) the energy $E_0(S^-)$ of the neutral S calculated at the geometry of the anion radical S^- . Thus, the reorganization energy $\lambda_i(S)$ becomes

$$\lambda_i(S) = \frac{1}{2} [E_-(S) - E_-(S^-) + E_0(S^-) - E_0(S)] \quad (7)$$

A similar approach was used to calculate the reorganization energy for the HT process.

2.3 Quantum chemical calculations

We used the DFT method with the B3LYP, M05 [18, 19] and MPWB1K [20] hybrid functionals and the basis set 6-31++G**. Some additional calculations were also carried out with smaller basis sets. Radical-anion and radical-cation states were calculated with the unrestricted DFT scheme. The details of the CASSCF and CASPT2 calculations on the DNA base stacks are given in Refs. [21, 22]. The DFT and CASSCF calculations were carried out using the program Gaussian03 [23] and the CASPT2 calculations with Molcas 5.4 [24].

It is well known that extended basis sets supplemented with diffuse functions are required to properly describe molecular anions using quantum chemical calculations. However, if a neutral molecule has large dipole moment (as for instance nucleobases), inclusion of diffuse functions may negatively affect the computational results for the radical anion. This is because two types of radical-anion

states are found for such molecules: the “usual” valence state with the negative charge delocalized over the molecule and the dipole-bound state, in which the excess electron is located far outside the molecule [25, 26]. Using an extended basis set containing diffuse functions will stabilize the ion-dipole states leading thereby to contamination of the valence state with the dipole-bound state. It has been shown that HF and DFT calculations without diffuse functions produce reasonable estimates of the EAs and electron transfer parameters for nucleobases and their stacks, while inclusion of diffuse functions in the calculation leads to less accurate or even wrong results [27, 28]. Because aromatic hydrocarbons are nonpolar molecules with small or zero dipole moment, extended basis sets must be employed to describe the electronic properties of their radical-anion states. On the other hand, such bases sets should be used with care when treating valence states of radical anions formed by very polar molecules.

3 Results and discussion

3.1 Polycyclic aromatic hydrocarbons

As noted in Sect. 1, oligoacenes are currently considered as a very promising material for organic electronics [1, 29]. Also, discotic materials based on triphenylene are of great interest [1]. In this section, we consider how electronic properties of polycyclic aromatic compounds depend on the molecular structure. As is well known, the equilibrium geometry of a molecule changes by the electron detachment and electron attachment processes due to vibronic coupling. The difference of vertical and adiabatic ionization potentials (or electron affinities) gives the internal reorganization energy λ_+ and λ_- accompanying the detachment and attachment processes. Vibronic coupling in oligoacenes has been previously considered in several theoretical and experimental studies [1].

Let us start with the results listed in Table 1. Two hybrid functionals, B3LYP and M05, were employed for the calculations. Relatively small changes of structural parameters are found by passing from the neutral species to the corresponding radical cation and anion. In particular, all species remain planar by both detachment and attachment of an electron, with the exception of [4]helicene, which is already nonplanar for the neutral state.

The B3LYP and M05 estimates of the reorganization energy are in good agreement, with the M05 values being consistently somewhat larger than those from B3LYP. Previously it has been shown that DFT calculated values of λ_+ and λ_- increase with the amount of the HF exchange contribution included in the hybrid functionals [30]. As the contribution of exact exchange in B3LYP and M05 is

Table 1 Reorganization energies λ_+ and λ_- (in meV) for electron detachment and electron attachment calculated using the B3LYP and M05 functionals and the 6-31++G** basis set

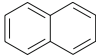
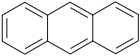
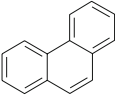
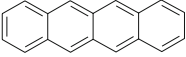
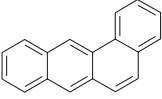
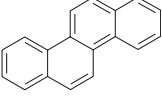
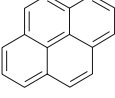
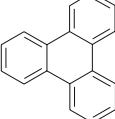
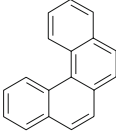
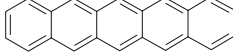
Molecule	λ_+ B3LYP	λ_+ M05	λ_- B3LYP	λ_- M05
Naphthalene 	89	98	116	124
Anthracene 	67	78	96	102
Phenanthrene 	107	118	152	157
Tetracene 	58	65	81	86
Tetraphene 	69	78	90	97
Chrysene 	79	94	102	109
Pyrene 	74	87	105	113
Triphenylene 	89	104	114	124

Table 1 continued

Molecule	λ_+ B3LYP	λ_+ M05	λ_- B3LYP	λ_- M05
[4]Helicene 	63	85	77	91
Pentacene 	47	57	67	74

20 and 28%, respectively, the found trend $\lambda(\text{M05}) > \lambda(\text{B3LYP})$ is in line with the conclusion derived by Sanchez-Carrera et al. [30]. Recently, experimental values of λ_+ of several oligoacenes were derived from gas-phase photoelectron spectroscopy measurements [31]. For anthracene, tetracene and pentacene, λ_+ is found to be 69.7, 58.8 and 49.6 meV, respectively [31]. Comparison of these data with our estimates (Table 1) suggests that B3LYP provides more accurate reorganization energies than M05. Because of that, in the following discussion, we will only refer to the B3LYP values. As seen from Table 1, λ_+ changes from 89 meV in naphthalene to 47 meV in pentacene becoming smaller with the size of the system. Note that the reorganization energy of a molecule within the crystal may be smaller than that found for isolated systems due to delocalization of the excess charge [32]. For instance, λ_+ of naphthalene within a shell of nearest neighbors is predicted two times smaller than λ_+ in isolated molecule [32]. As seen from Table 1, the reorganization energy is quite different for isomers or for compounds with the same number of aromatic rings. For instance, λ_+ in anthracene is smaller than that of phenanthrene by a factor of 1.5. For four-ring systems, λ_+ values increase in the order tetracene < [4]helicene < tetraphene < pyrene < chrysene; the values for chrysene are higher than those for tetracene by a factor of 1.5. Thus, linear acenes have smaller reorganization energies than kinked arenes.

Similar results are obtained for electron attachment. High-level calculations of EA of several polyacenes have been reported recently [33]. In particular, it was shown that naphthalene has negative EA values. Also, our calculations predict the adiabatic and vertical electron affinities (EA) of

naphthalene to be negative, -0.24 eV (the excess electron is unbound in the radical anions). Therefore, the calculated value of λ_- (0.12 eV) cannot be considered as quite reliable.

In all cases, the calculated values of λ_- for oligoacenes and related compounds are found to be remarkably larger than λ_+ . This is in line with experimental findings that the hole mobility of most organic semiconductors is at least an order of magnitude higher than the excess electron mobility [1]. However, there are few systems such as perylene that have larger excess electron mobilities than hole mobilities [34]. Assuming that the electronic couplings for HT and EET between π -stacked aromatic molecules are similar (see below), the ratio $R = \lambda_-/\lambda_+$ of the electron and hole mobilities can be estimated as $R = \exp(\lambda_- - \lambda_+/4kT)$ using Marcus equation (Eq. 1). For tetracene and pentacene, R is ca. 1.5; similar R values are obtained for most molecules listed in Table 1; the largest value, $R = 2.4$, is found for phenanthrene. The fact that experimental hole mobilities are essentially higher than electron mobilities (at least an order of magnitude) cannot be explained solely by the difference in λ_+ and λ_- . In some cases, it was possible to observe a correlation between decreasing reorganization energy and increased field effect mobility [35].

The reorganization energy for the aromatic systems is quite small, less than 100 meV (see Table 1) and similar in magnitude to intermolecular electronic coupling between subunits in the materials, the localization of the excess charge on a single site appears to be unlikely.

The internal reorganization energies λ_+ and λ_- are determined by interatomic distance variations caused by electron detachment and attachment, respectively. It would be helpful to have a simple electronic index derived from electronic structure calculation of the neutral system that could be used to predict the λ_+ and λ_- values. We have attempted to define a proper global index making use of the excess charge atomic populations and overlap populations described by Eqs. 3–6.

We have defined two *global atomic excess charge* indexes as

$$Q_+ = \sqrt{\sum_A (q_A^{\text{HOMO}})^2}, \quad Q_- = \sqrt{\sum_A (q_A^{\text{LUMO}})^2} \quad (8)$$

which take into account the degree of atomic charge reorganization upon electron detachment or attachment, respectively.

The values of these indexes calculated for the set of polycyclic aromatic hydrocarbons are listed in Table S1 (see the Supporting information). Three different population analysis techniques have been used, namely, Mulliken, fuzzy atom and Hirshfeld. The values obtained using Mulliken excess charges are always larger than the 3D-space-based ones, indicating larger local (atomic)

excess charges. The correlation between Q_+ index and λ_+ energies is very poor in all cases. Slightly better but still unsatisfactory is the correlation between Q_- and λ_- . The Hirshfeld charges provide the best agreement, whereas Mulliken is the worst case.

It is worth to note that Mulliken-based charges (and excess charges) may result in spuriously large values, specially when using large basis sets. This has been the case specially for chrysene and pyrene, for which Mulliken atomic charges beyond 11.5e1 have been obtained. Such spurious charge values given by the Mulliken approach are deeply connected with near-linear dependencies in the basis set. In fact, a rather problematic situation is quite frequent with standard electronic structure software such as Gaussian03 with default options. The eigenvectors of the basis set overlap matrix with eigenvalues below a given threshold (typically 10^{-6}) are discarded and hence the dimension of the orthogonal basis set is reduced. The smaller the threshold for the elimination of basis functions the more “chemical” and closer to those obtained with 3D methods the Mulliken charges become. However, as a result the actual number of basis functions used in the calculation can be reduced significantly, which translates into poorer energies and even loss of the symmetry of the wave function and the respective Mulliken atomic charges. The main advantage of the 3D-based population methods is that they do not suffer from these problems and are much more robust and reliable. For instance, the atomic charges obtained with fuzzy atom and Hirshfeld approaches for the set of PAH’s are always below 10.25e1, in better agreement with chemical expectation.

Based on a simple physical assumption (correlation between the bond length l and electronic density on the bond, the contribution of a given mode is proportional to Δl^2), we suggest as alternative to the atomic excess charges the use of bond excess charges and introduce the global bond excess charge indices B_+ and B_- as

$$B_+ = \sqrt{\sum_{A<B} (q_{AB}^{\text{HOMO}})^2}, \quad B_- = \sqrt{\sum_{A<B} (q_{AB}^{\text{LUMO}})^2} \quad (9)$$

where the sum is taken over all distinct atomic pairs and q_{AB}^{HOMO} and q_{AB}^{LUMO} are the HOMO and LUMO contributions to the overlap density between the atomic pair AB , as defined in Eqs. 4 and 6. These indexes describe changes in bonding interactions’ (electron sharing) strengths by electron attachment or detachment and therefore can better account for the reorganization effects in the bonding.

The calculated indexes for the set of PAH’s using different overlap population methods are given in Table S2 (see the Supporting information). Again the Mulliken values are very large compared to the fuzzy atom of Hirshfeld values, specially for the B_- index. Whereas no correlation is observed between the B_+ and λ_+ , in the case

of the electron detachment (B_- and λ_-) the correlation is significant ($r^2 \sim 0.7$). In fact, when using minimal basis sets global bond excess charge indexes correlate fairly well with the reorganization energies (results not reported), indicating again that Mulliken charges may be strongly basis set dependent. In the case of fuzzy atom and Hirshfeld methods, both B_+ and B_- indices show overall good trend with r^2 values larger than 0.5. Hirshfeld values of the bond indices are systematically larger than the fuzzy atom ones. This can be inferred from the fact that Hirshfeld atoms are slightly polar and tend to provide small charges and consequently larger overlap populations.

Thus, we have observed that bond excess charge is a better descriptor for the reorganization energy than atomic excess charge. However, both indices describe electron charge, either atomic or shared, and are to be compared with an energetic quantity. This indicates that it is probably necessary to introduce an energetic counterpart into the bond excess charge index, in order to account not just for how much shared electrons redistribute upon electron attachment or detachment but also for the energetic cost of this redistribution. In this line, we have finally introduced a new energy-based index making use of the Fock matrix. One can define an energetic parameter for each atomic pair analogous to the overlap population using

$$\begin{aligned} e_{AB}^{\text{HOMO}} &= 2 \sum_{\mu \in A} \sum_{\nu \in B} c_{\mu, \text{HOMO}} F_{\mu\nu} c_{\nu, \text{HOMO}}^* \\ e_{AB}^{\text{LUMO}} &= 2 \sum_{\mu \in A} \sum_{\nu \in B} c_{\mu, \text{LUMO}} F_{\mu\nu} c_{\nu, \text{LUMO}}^* \end{aligned} \quad (10)$$

where $F_{\mu\nu}$ are the elements of the Fock (Kohn–Sham in the DFT case) matrix in the atomic orbital basis. Using Eq. 10, one can define the corresponding energetic counterpart of the global bond excess charge indexes for electron detachment and attachment

$$EB_+ = \sqrt{\sum_{A < B} (e_{AB}^{\text{HOMO}})^2}, \quad EB_- = \sqrt{\sum_{A < B} (e_{AB}^{\text{LUMO}})^2} \quad (11)$$

In this case, we have only used Mulliken type indexes. In the case of a 3D-based index, a numerical integration of the Fock matrix elements over pair of atomic domains must be carried out, which would formally involve very costly two-electron numerical integrations.

In Table S3, we report the values obtained for the indexes in Eq. 11 and in Fig. 1 the corresponding correlations with the reorganization energies λ_+ and λ_- . The results are quite satisfactory. First, the correlation for the λ_+ energies dramatically improves from essentially zero with the B_+ index to 0.80 with the energetic counterpart EB_+ . In the case of the electron attachment process, the B_- and EB_- indexes perform similarly well, being slightly superior the latter. This could be justified taking into

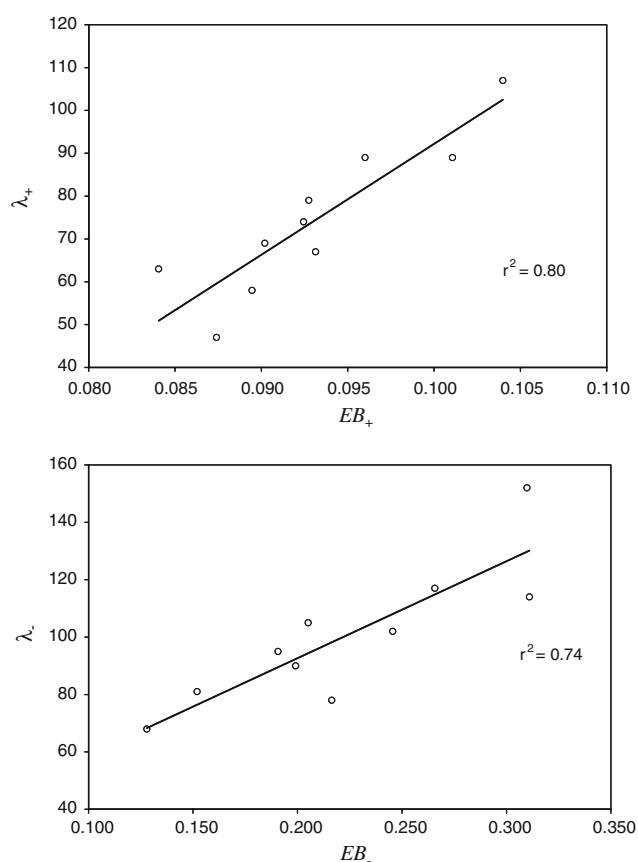


Fig. 1 Correlation between the index EB_+ and reorganization energy λ_+ for the HT process (upper panel) and between the index EB_- and λ_- reorganization energy for the EET (lower panel). Reorganization energies in meV

account that the Fock matrix has explicit dependence on the occupied orbitals and, therefore, the energetic contribution of the HOMO orbital is expected to be better described than for the LUMO. Another improvement of the energetic indexes over the electronic ones is that the problems associated to the Mulliken partitioning seem to be less important now. Of course, this fact deserves further studies of the basis set effects which are beyond the scope of this work. We believe that this new energetic index is a promising tool for the semi-quantitative prediction of reorganization energies associated to HT and EET processes. Further studies of basis set robustness and application to a wider set of chemical compounds are under way in our laboratory.

3.2 ECD in π stacks

In Table S4 (Supporting information), we provide the electronic couplings for HT and EET (V_+ and V_-) in symmetric dimers of the aromatic molecules with the intermolecular distance of 3.5 Å. The electronic coupling

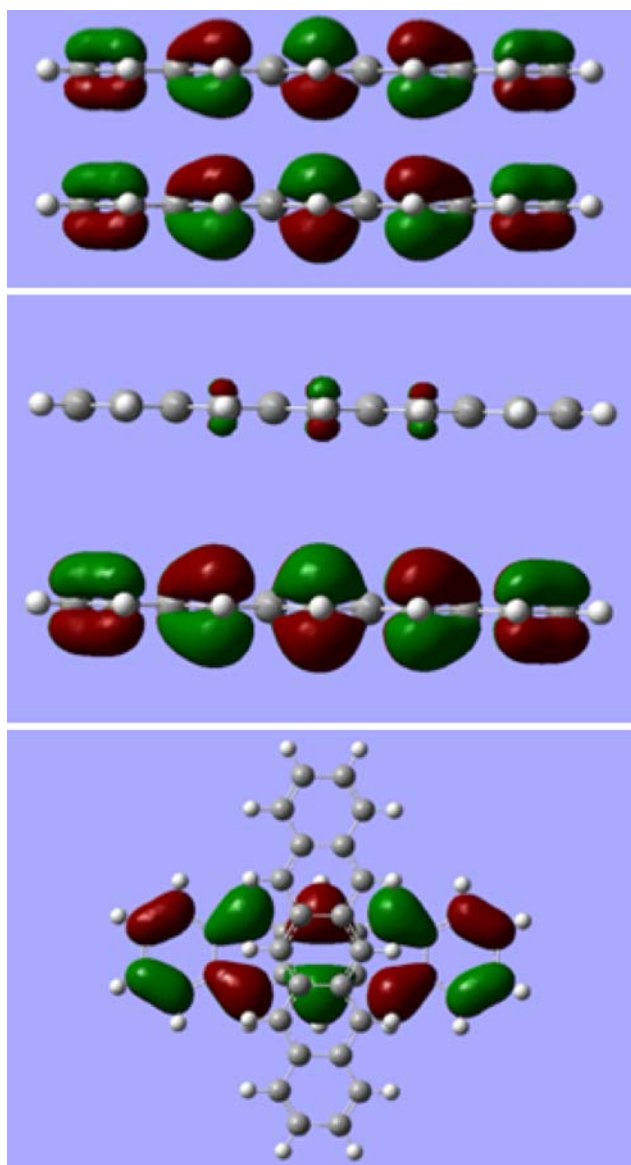


Fig. 2 HOMO orbitals of the pentacene dimer with parallel arrangement of subunits at the distance of 3.5 Å (at the *top*) and 5 Å (in the *middle*) and with perpendicular arrangement of molecules at the distance of 3.5 Å (at the *bottom*)

for symmetry-equivalent donor and acceptor can be estimated as one-half of the energy gap Δ between adiabatic states. As HOMO and LUMO orbital energies within HF and DFT provide a good approximation for estimating the HT and EET coupling, respectively [21, 22, 36], these matrix element can be well estimated as one-half of the corresponding orbital energy splitting. One considers HOMO- k ($k = 0, 1, \dots$) for hole transfer and LUMO+ k for EET. What is important is that the pairs of related orbitals should represent + and - combinations of states localized on monomers. In many cases (but not always) the

orbital energies of HOMO and HOMO-1 in neutral symmetrical dimers can be used to derive V_+ and those of LUMO and LUMO+1 for V_- . Analysis of the shape of the molecular orbitals in dimers is necessary to obtain correct estimates of the couplings.

For instance, in the dimers of phenanthrene, tetraphene, chrysene and [4]helicene, HOMO and HOMO-2 (not HOMO-1) should be considered to calculate V_+ , whereas energies of LUMO and LUMO+2 (not LUMO+1) determine V_- . The HOMOs of the phenanthrene dimer are depicted in Figure S1. As seen, the orbital pairs, HOMO and HOMO-2 and LUMO and LUMO+2, represent symmetric and antisymmetric combinations of interest; HOMO-1 and LUMO+1 cannot be employed in combination with HOMO and LUMO, respectively, to derive the coupling matrix elements. The estimated values of V_+ and V_- are very similar (Table S4) and amount to 350 meV. Note that the couplings decrease exponentially with the increasing distance between monomers. Furthermore, distortion of symmetric structure may considerably reduce the overlap between MO of monomers and thereby strongly affect the corresponding couplings. Thus, the estimated values of V_+ and V_- represent upper limits for stacked aromatic molecules.

As already noted in Sect. 1, the ECD in stacks is determined by interplay between electronic coupling and reorganization energy. Let us compare hole distribution in two pentacene dimers. In the complexes, one subunit has the molecular geometry of neutral pentacene, while the other corresponds to the radical cation, with an intermonomer distance of 3.5 Å. This means that the effect of internal reorganization by electron detachment is taken into account. The second complex is obtained from the first one by rotation of one pentacene by 90°. As can be seen, in the first complex the charge is delocalized over both pentacenes, while in the second dimer the charge is almost completely confined to single subsystem. This is because V_+ sharply decreases by the rotation of the subunit. Note that such a conformational transition is associated with a small change in the total energy. Thus, the ECD in the complex is considerably affected by conformational changes. This observation is largely supported by the third example, in which the distance has been increased from 3.5 to 5 Å. As can be seen in Fig. 2, now the charge is mainly localized on one of the monomers. A similar picture is obtained for the radical-anion state of the complexes. The excess electron is delocalized over the system in the complex with parallel pentacenes and localized on one unit in the dimer with the perpendicular arrangement of the subunits. Such an alteration of ECD is due to the small reorganization energies associated with electron detachment and attachment processes.

3.3 Fullerene–tweezers complex

Usually the π interaction in molecular aggregates is considered for planar aromatic molecules. Let us briefly discuss a quite different system consisting of fullerene and buckycatcher (tweezers) (Fig. 3) which has been recently reported [37]. The complex is formed due to the aromatic–aromatic interaction between the convex surface of the fullerene and the concave faces of corannulene subunits of the tweezers. Such a type of organic systems is of potential interest in the design of nanoelectronics devices. Very recently, Zhao and Truhlar [38] studied the geometries and binding energies of the complex using DFT with new functionals that include an accurate treatment of medium-range correlation energy. The gas-phase free energy of the complex formation is found to be -6.7 kcal/mol. Injection of an excess electron into the complex yields a radical-anion system.

Let us consider excess electron distribution in the complex. The electronic coupling of the subunits in the system is ca. 100 meV [39]. For fullerene and the tweezers, the B3LYP reorganization energies λ_- are 65 and 80 meV. Unlike pentacene dimers, where the donor and acceptor sites are equivalent (symmetric arrangement of the subunits) or very similar (nonsymmetric structures), the ionization potential and EA of subunits in the complex

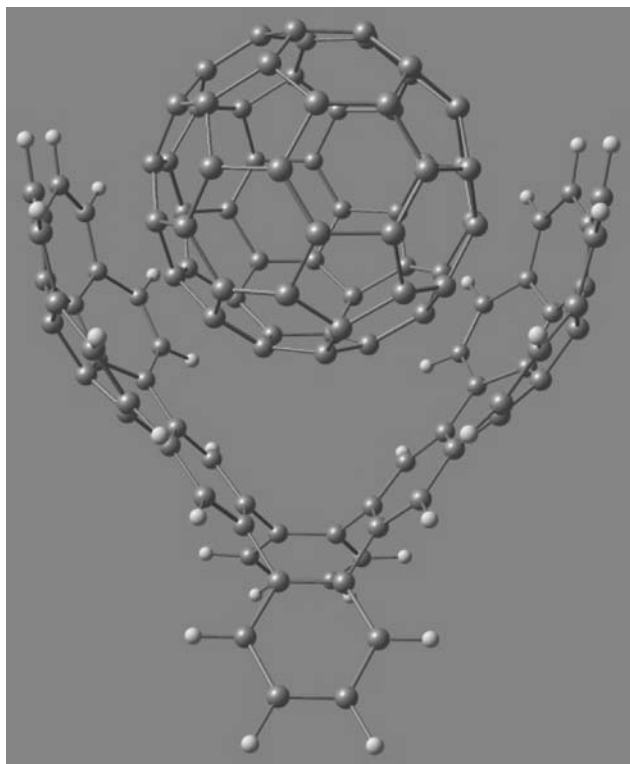


Fig. 3 Structure of the fullerene–tweezers complex

essentially differ. C_{60} is a better trap for excess electron than the tweezers; the EA difference is estimated to be 1.8 eV. If donor and acceptor in a system are different, ECD depends strongly on the energy gap $\Delta\varepsilon^0$ between these sites [14, 39]. Localization of the excess charge will strongly increase with $|\Delta\varepsilon^0|$. Using estimated values of $\Delta\varepsilon^0$, V and λ ($\lambda = \lambda_-(C_{60}) + \lambda_-(\text{tweezers}) = 145$ meV), one derives that the excess electron in the complex should be almost completely (99%) confined to C_{60} .

3.4 ECD in DNA stacks

In DNA, aromatic nucleobases (adenine A, cytosine C, guanine G, and thymine T) form π stacks with the inter-base distance of 3.4 Å. One may expect that the excess charge will be quite delocalized in the stack as found, e.g., in oligocene dimers. Moreover, some computational studies predict a delocalized ECD in DNA [40]. In this section, we report the results of gas-phase CASSCF and CASPT2 calculations that were carried out as benchmarks for the coupling elements for HT and EET between two stacked DNA nucleobases in their B-DNA conformation. These results strongly suggest that ECD should be strongly localized within DNA π stacks. Here, we focus on how the ionization energies of the isolated bases and conformational effects affect the charge distribution on the two nucleobases. The calculations show that for HT and EET the charge distribution is mainly governed by the ionization potentials (IP) and electron affinities (EA), respectively. Conformational effects on the charge distribution are smaller and relevant for homodimers or cases where the bases have the similar site energies.

The Mulliken charge distribution and the differences in the ionization potentials are summarized in Table 2. We have studied π stacks of different bases at their regular B-DNA conformation (inter-plane separation 3.38 Å), using the atomic coordinates from high-resolution X-ray and neutron studies [41]. The charges have been calculated at the CASSCF level of theory, and the ionization energies at the CASPT2 level. As discussed in Refs. [21, 22], the CASSCF ECD is reliable for all base pairs except for the radical-anion states of stacks CT and TC because of the wrong relative electron affinities at that level. Thus, for the CT and TC pairs, the charges have been obtained from the perturbationally modified wave function (PM-CASCI) derived from the multi-state CASPT2 effective Hamiltonian [22].

For different base pairs X and Y, the stacks XY and YX differ in their conformation and have different properties. Therefore, it is possible to compare the effect of the difference in ionization energies on the charge localization with the effect of electrostatic interactions, which depend on the conformation. In most cases, the hole is localized on

Table 2 Charge distribution, difference in ionization energies (ΔIE) and energy gap between ground and excited states (ΔE) for stacked nucleobase pairs

Hole transfer				
XY	q_X	q_Y	$\Delta IE_{\text{CASPT2}}$	ΔE_{CASPT2}
GA	0.99	0.01	0.41	0.56
AG	0.02	0.98	0.41	0.34
GT	0.99	0.01	1.09	1.18
TG	0.01	0.99	1.09	0.80
GG	0.98	0.02	0.00	0.39
AA	0.01	0.99	0.00	0.10
Excess electron transfer				
XY	q_X	q_Y	$\Delta AE_{\text{CASPT2}}$	ΔE_{CASPT2}
TA	-0.99	-0.01	0.51	0.44
AT	-0.04	-0.96	0.51	0.49
TG	-1.00	0.00	1.05	0.58
GT	-0.96	-0.04	1.05	1.04
TC ^a	-0.97	-0.03	0.17	0.10
CT ^a	-0.64	-0.36	0.17	0.40
TT	-0.98	-0.02	0.00	0.16

Charges calculated at the CASSCF(11,12)/6-31G* (HT) and CASSCF(13,12)/6-311G* (EET) level of theory; ionization energies of the isolated bases calculated at the CASPT2 level (see Refs. [21, 22] for further computational details)

$$\Delta IE = |IP_Y - IP_X|$$

$$\Delta AE = |EA_Y - EA_X|$$

^a Charges and energies calculated at the MS-CASPT2 level of theory

the base with the lowest ionization potential (G for GA and GT pairs) and the excess electron on the base with the highest electron affinity (T for TA and TG pairs), irrespective of the conformation. The only exception is the CT stack, where the charge is preferentially localized on C in spite of its lower electron affinity. This is due to the close electron affinities of thymine and cytosine, in which case the electrostatic interactions can reverse the trend dictated by the ionization energies. Turning to the XX stacks, in all studied cases (HT for AA and GG, and EET for TT), the electrostatic interactions induce a localization of the charge on one of the bases.

Further insight into the electrostatic effects on the charge localization can be obtained in the frame of a two-state model for charge transfer. In this model, the ground and excited states correspond to the states where the charge is localized on one or the other base. Most of the stacked pairs adjust to this model (>95% charge localization on one of the bases), and in the excited state the charge distribution is simply reversed with respect to the ground state. In this model, the charge is localized on the base that has the lowest ionization energy. Electrostatic effects on the

charge distribution can be understood as changes in the ionization energies of the stacked bases induced by their neighbor, and in this context one can speak of ionization energies *in the stack*. This is not a physical magnitude, but it is an approximation to the potentials of the ‘diabatic’ donor and acceptor states, V_d and V_a . If the relative ionization energies of the bases in the stack are equalized or their sign is changed with respect to the gas-phase energies, the charge will delocalize along the two bases or localize on the base with the highest gas-phase ionization energy.

To estimate how much the ionization energies in the stack differ from the gas-phase values, it is useful to examine the energy gap between the ground and the excited states, ΔE . In the two-state model, ΔE (the ‘adiabatic’ energy gap) can be obtained from the energies of the ‘diabatic’ donor and acceptor states, ε_d and ε_a , and the electronic coupling between donor and acceptor V_{da} :

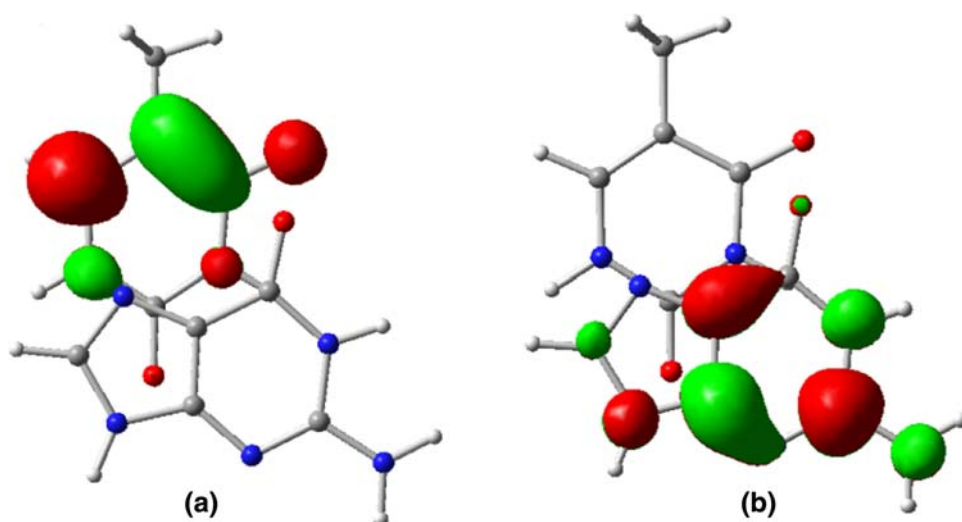
$$\Delta E = \sqrt{(\Delta\varepsilon)^2 + 4V_{da}^2} \approx \Delta\varepsilon \quad (12)$$

$$\Delta\varepsilon = |\varepsilon_a - \varepsilon_d|$$

In the present case, the electronic coupling is at least one order of magnitude smaller than the adiabatic energy gap ΔE , and ΔE should be well approximated by $\Delta\varepsilon$, which in turn can be understood as the difference between the ionization energies or EAs of the two bases in the stack.

Following this argument, comparison of ΔEA and ΔE for the studied pairs shows substantial differences for the TG pair. This suggests that the neighboring base has a substantial effect on the electron affinities of either T or G, or both. In particular, the energy of the T^0G^- state (the excited ‘adiabatic’ state or the acceptor ‘diabatic’ state) relative to the T^-G^0 state in the stack (Fig. 4) is stabilized by approximately 0.5 eV with respect to the gas phase (from 1.05 to 0.58 eV). The origin of this stabilization has been studied by recalculating the electron affinities of T and G in the presence of the neighboring base, simulated by the charges fitted to the electrostatic potential [42] located on their respective atoms. In the TG conformation, the electron affinity of T is lowered by 0.42 eV by the charge distribution corresponding to G, while the electron affinity of G is lowered by 0.11 eV by the charges of T. These calculations, therefore, predict a net stabilization of the T^0G^- state by 0.3 eV, which is in agreement with the trend obtained from comparing ΔEA and ΔE (stabilization by 0.5 eV). We have tried to find a ‘chemical’ explanation for this trend by examining the semi-occupied orbitals for the two bases in the stack (CASSCF active-space orbitals with occupation 1.00), but there seems to be no clear-cut explanation. For the remaining heterodimers, the differences between ΔIE (ΔEA) and ΔE are smaller, which indicates that the effect of stacking on the ionization energies is small, or that the effects on each of the bases cancel each other.

Fig. 4 Charge distribution in TG for EET shown with the semi-occupied orbitals for the two states. **a** Ground state ($T^{\ominus}G^{\ominus}$), **b** excited state ($T^{\ominus}G^{\ominus}$)



In summary, the CASSCF and CASPT2 results show that the excess charge localization in stacked nucleobases mainly follows the trend of the ionization energies (for radical cations) and electron affinities (for radical anions). For HT, the charge tends to localize on guanine, which has the lowest ionization potential, whereas for EET, the trend is towards localization on thymine, which has the highest electron affinity. However, due to the electrostatic interactions with neighboring bases in the stack, the ionization energies and electron affinity are essentially affected, and this may induce delocalization of the excess charge or, on the contrary, its localization on a single base. This has been observed for the pair formed by C and T in EET. Moreover, the estimation of the ionization energies of T and G in the TG stack shows that the base pairing can change the ionization energy up to 0.4 eV. Thus, it is conceivable that in cases other than C and T, at suitable conformations, the neighboring effects may induce charge localization on the less favored base in the gas phase.

3.5 Charge delocalization in amino acids: histidine

In polypeptides and proteins, conformational dependence of ECD appears to be even more complicated than organic and DNA stacks because considerable alterations of ECD may occur already within amino acids (AA). Besides charge transfer characteristics, the ECD strongly affects such properties as fragmentation of AA, proton donor and acceptor properties of polypeptides, the strength of hydrogen bonding between subunits and some other properties. Because of that, an analysis of ECD in AA is of special interest.

For non-aromatic amino acids, it was shown that the ionization takes place at the amino group of the backbone, which becomes more planar and acidic [43]. However, for aromatic AAs, the hole is mainly localized on the aromatic

ring, as the ionization potential of the ring is lower than that of the NH_2 group. The localization of the excess charge depends on the aromatic character of the side chain and, what is more important, on the conformation of the amino acid.

Histidine radical cation was studied by Gil et al. [44] using the hybrid B3LYP and hybrid-meta MPWB1K functionals with 6-31++G**. Histidine with an imidazole ring at the side chain has two different tautomers ($\text{N}^{\delta^2}\text{-H}$ and $\text{N}^{\delta^1}\text{-H}$) in which different nitrogen atoms are protonated. A conformational search was done for the radical-cation states of both tautomers. The whole palette of conformers is presented elsewhere [44]. Here, we consider only several structures that represent typical situations for ECD in histidine (see Fig. 5). The first structure HisIII δ (+)1 has a hydrogen bond (HB) between the proton of the side chain and the NH_2 group of the backbone. HisIV ϵ (+)2 has two HBs, one due to the interaction of NH_2 with CO and the other formed between the same NH_2 group with N of the side chain. The last structure, HisIII ϵ (+)1, is characterized by 2-center-3-electron interaction between the backbone CO and the N of the side chain.

Table 3 compares the charge and spin density distribution derived from natural population analysis of three conformers calculated using B3LYP and MPWB1K. It is known that B3LYP tends to overestimate the stability of structures with 2-center-3-electron interactions [45], such as HisIII ϵ (+)1, which is the most stable structure at B3LYP level, while MPWB1K predicts HisIII δ (+)1 to be of the lowest energy (relative energies of the conformers are found to be within 2.5 kcal/mol).

As found in previous studies, ionization of aromatic amino acids leads generally to a hole state which is localized on aromatic ring. For His, however, ECD depends on the structure of the radical cation. As can be seen from Fig. 5, ECD in HisIII δ (+)1 and HisIII ϵ (+)1 is

Fig. 5 Optimized geometries (distances are in Å) of the lowest energy conformers of the histidine radical cation (*upper panel*) and their singly occupied molecular orbitals calculated at the MPWB1K/6-31++G** level

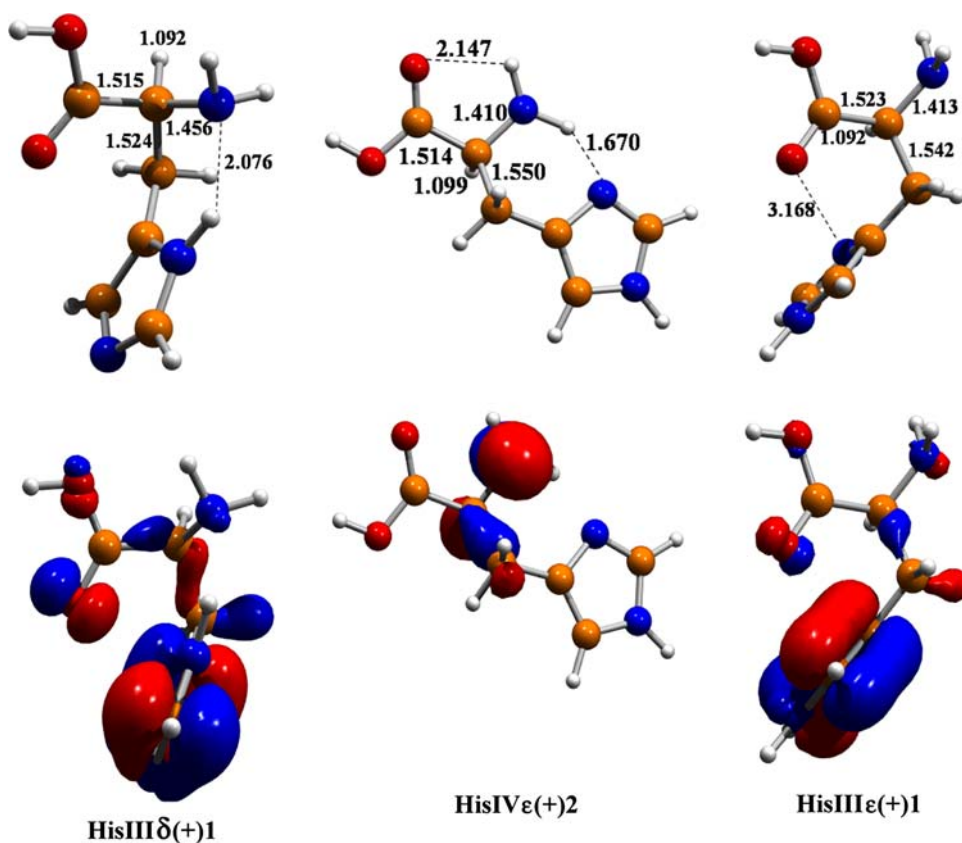
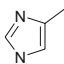


Table 3 Excess charge distribution//spin densities calculated with MPWB1K/6-31++G** and B3LYP/6-31++G** (in italics)

	NH ₂	COOH		CH
HisIIIδ(+)-1	-0.10//0.00 <i>-0.02//0.07</i>	0.08//0.03 <i>0.13//0.13</i>	0.90//0.96 <i>0.72//0.72</i>	0.12//0.01 <i>0.17//0.08</i>
HisIVε(+)-2	0.58//0.89 <i>0.45//0.43</i>	0.10//0.0 <i>0.33//0.51</i>	0.22//0.07 <i>0.09//0.02</i>	0.10//0.07 <i>0.13//0.04</i>
HisIIIε(+)-1	-0.04//0.03 <i>0.07//0.17</i>	0.10//0.11 <i>0.13//0.15</i>	0.81//0.82 <i>0.66//0.65</i>	0.14//0.03 <i>0.14//0.03</i>

MPWB1K data are adopted from Ref. [44]

typical for aromatic amino acids; the excess charge is localized on the ring. For conformations with a HB between the NH₂ and the N of the side chain, the ECD is similar to that in the non-aromatic amino acids: the excess charge is localized on NH₂ of the backbone.

It is known that B3LYP tends to overestimate the delocalization of charge and spin density while MPWB1K provides more localized ECD. For HisIIIδ(+)-1 and HisIIIε(+)-1 (Table 3), MPWB1K suggests that the hole density is almost completely confined to the imidazole

ring, while B3LYP predicts the hole charge to be quite delocalized. The same trend is followed by HisIVε(+)-2, where the B3LYP hole density is “artificially” spread over NH₂ and COOH. The different pictures for ECD obtained within MPWB1K and B3LYP are translated into different properties of HisIVε(+)-2. For instance, MPWB1K clearly indicates intramolecular proton transfer whereas B3LYP results are interpreted as hydrogen abstraction [44].

4 Concluding remarks

We have considered several molecular systems with different types of ECD. The analysis of ECD within these species has been performed in terms of key charge transfer parameters (reorganization energy, electronic coupling and CT energy) calculated with DFT and ab initio methods. ECD in π stacks of polycyclic aromatic hydrocarbons and its dependence on mutual arrangement of subunits are examined. In general, ECD in organic materials should be essentially delocalized because of relatively large electronic couplings between molecules and small CT and reorganization energies. In conformational region, where the coupling is small, e.g. perpendicular arrangement of pentacenes, structural fluctuations will lead to substantial variation of ECD (from completely delocalized to localized

charge and spin densities). However, in the fullerene–tweezers complex where the donor and acceptor sites are quite different (and therefore, the energy gap between the corresponding diabatic states is significant) the excess charge is quite localized. In DNA, the excess charge is found to be confined to a single base. Even in homogeneous stacks consisting of the same base, ECD should be localized because of the large reorganization energy. Interestingly, low conformational changes in polypeptides may cause essential redistribution of the excess charge density within amino acids (excess charge alternates between a side aromatic ring and the backbone). Such an effect can be important for CT in proteins.

Acknowledgments This work has been financially supported by the Spanish Ministerio de Educación y Ciencia Projects no. CTQ2005-04563, CTQ2005-08797-C02 and CTQ2008-03077/BQU. J.P. thanks the MEC for the Ramón y Cajal contract.

References

1. Coropceanu V, Cornil J, Filho DA, Olivier Y, Silbey R, Bredas JL (2006) *Chem Rev* 106:926
2. Walzer K, Maennig B, Pfeiffer M, Leo K (2006) *Chem Rev* 106:1233
3. Shirota Y, Kageyama H (2007) *Chem Rev* 107:953
4. Günes S, Neugebauer H, Sariciftci NS (2007) *Chem Rev* 107:1324
5. Shuster GB (2004) Long-range charge transfer in DNA. In: *Topics in current chemistry*, vols. 236–237. Springer, Berlin
6. Ratner MA (2002) *Mater Today* 5(2):20
7. Ratner MA, Jortner J (1997) *Molecular electronics*. Marcel-Dekker, New York
8. Bredas JL, Beljonne D, Coropceanu V, Cornil J (2004) *Chem Rev* 104:4971
9. Bredas JL, Calbert JP, DAdS Filho, Cornil J (2002) *Proc Natl Acad Sci USA* 99:5804
10. Marcus RA, Sutin N (1985) *Biochim Biophys Acta* 811:265
11. Newton MD (1991) *Chem Rev* 91:767
12. Marcus RA, Sutin N (1985) *Biochim Biophys Acta* 811:265
13. Olofsson J, Larsson S (2001) *J Phys Chem B* 105:10398
14. Voityuk AA (2005) *J Phys Chem B* 109:10793
15. Parson WW, Chu ZT, Warshel A (1998) *Biophys J* 74:182
16. Bader RFW (1990) *Atoms in molecules—a quantum theory*. Oxford University Press, Oxford
17. Hirshfeld FL (1977) *Theor Chim Acta* 44:129
18. Zhao Y, Schultz NE, Truhlar DG (2005) *J Chem Phys* 123:161103
19. Zhao Y, Schultz NE, Truhlar DG (2006) *J Chem Theory Comput* 2:364
20. Zhao Y, Truhlar DG (2004) *J Phys Chem A* 108:6908
21. Blancafort L, Voityuk AA (2006) *J Phys Chem A* 110:6426
22. Blancafort L, Voityuk AA (2007) *J Phys Chem A* 111:4714
23. Frisch MJ et al (2008) *Gaussian 03E*. Gaussian, Pittsburgh
24. Karlström G, Lindh R, Malmqvist PÅ, Roos BO, Ryde U, Veryazov V, Widmark PO, Cossi M, Schimmelpennig B, Neogrady P, Seijo L (2003) *Comput Mater Sci* 28:222
25. Adamowicz L (1993) *J Phys Chem* 97:11122
26. Al-Jihan I, Smets J, Adamowicz L (2000) *J Phys Chem* 104:2994
27. Li X, Cai Z, Sevilla MD (2002) *J Phys Chem A* 106:1596
28. Voityuk AA (2005) *J Chem Phys* 123:034903
29. Bendikov M, Wudl F, Perepichka DF (2004) *Chem Rev* 104:4891
30. Sanchez-Carrera RS, Coropceanu V, da Silva DA, Friedlein R, Osikowicz W, Murdey R, Suess C, Salaneck WR, Bredas JL (2006) *J Phys Chem B* 110:18904
31. Coropceanu V, Malagoli M, da Silva DA, Gruhn NE, Bill TG, Bredas JL (2002) *Phys Rev Lett* 89:275503
32. Datta A, Mohakud S, Pati SK (2007) *J Chem Phys* 126:144710
33. Hajgató B, Deleuze MS, Tozer DJ, De Proft F (2008) *J Chem Phys* 129:084308
34. Chesterfield RJ, McKeen JC, Newton CR, Ewbank PC, Da Silva Filho DA, Bredas JL, Miller LL, Mann KR, Frisbie CD (2004) *J Phys Chem B* 108:19281
35. Mas-Torrent M, Hadley P, Bromley ST, Ribas X, Tarres J, Mas M, Molins E, Veciana J, Rovira C (2004) *J Am Chem Soc* 126:8546
36. Felix M, Voityuk AA (2008) *J Phys Chem A* 112:9043
37. Sygula A, Fronczek FR, Sygula R, Rabideau PW, Olmstead MM (2007) *J Am Chem Soc* 129:3842
38. Zhao Y, Truhlar DG (2008) *Phys Chem Chem Phys* 10:2813
39. Voityuk AA, Duran M (2008) *J Phys Chem C* 112:1672
40. Conwell EM, Bloch SM, McLaughlin PM, Basko DM (2007) *J Am Chem Soc* 129:9175
41. Clowney L, Jain SC, Srinivasan AR, Westbrook J, Olson WK, Berman HW (1996) *J Am Chem Soc* 118:509
42. Besler BH, Merz KM, Kollman PA (1990) *J Comp Chem* 11:431
43. Gil A, Simon S, Rodríguez-Santiago L, Bertrán J, Sodupe M (2007) *J Chem Theory Comput* 3:2210
44. Gil A, Simon S, Sodupe M, Bertrán J (2008) *Chem Phys Lett* 451:276
45. Sodupe M, Bertrán J, Rodríguez-Santiago L, Baerends EJ (1999) *J Phys Chem A* 103:166